

Optical Monitoring of 3C 390.3 from 1995 to 2004 and Possible Periodicities in the Historical Light Curve

Jun Tao^{1,2}, Junhui Fan^{3,4}, Bochen Qian^{1,2}, and Yi Liu³

taojun@shao.ac.cn

ABSTRACT

We report V, R, and I band CCD photometry of the radio galaxy 3C 390.3 obtained with the 1.56-m telescope of the Shanghai Astronomical Observatory from March 1995 to August 2004. Combining these data with data from the literature, we have constructed a historical light curve from 1894 to 2004 and searched for periodicities using the *CLEANest* program. We find possible periods of 8.30 ± 1.17 , 5.37 ± 0.49 , 3.51 ± 0.21 , and 2.13 ± 0.08 years.

Subject headings: galaxies:photometry - methods:data analysis - galaxies:active - Seyfert galaxy: individual: 3C 390.3

1. Introduction

Active galactic nuclei (AGNs) can be divided into two classes: radio-loud and radio-quiet. A small subgroup of radio-loud AGNs have displayed flux variability on time scales ranging from hours to decades (see a review by Fan 2005). Examples of long-term variations can be found in the light curves of 3C 120 (Jurkevich et al. 1971), OJ 287 (Sillanpää et al. 1988), 3C 345 (Kidger et al. 1992), PKS 0735+178 (Pollock, 1975, Fan et al. 1997, Qian & Tao 2004), BL Lacertae (Fan et al. 1998), 3C 66A (Lainela et al. 1999), 3C 279 (Fan 1999), S5 0716+714 (Qian et al. 2002), Mrk 335 (Tao et al. 2004), PKS 1510-089 & MA 0829+047 (Liller & Liller 1975), B2 1101+38 (Miller 1975) and in various other radio-selected BL Lacertae objects (Fan et al. 2002).

¹Shanghai Astronomical Observatory, CAS, 80 Nandan Road, Shanghai, 200030, China

²Joint Institute for Galaxies and Cosmology, ShAO and USTC, CAS

³Center for Astrophysics, Guangzhou University, Guangzhou 510006, China

⁴Physics Institute, Hunan Normal University, Changsha, China

3C 390.3 ($z=0.0561$; Osterbrock et al. 1975) is a well-known broad-line radio galaxy with broad double peaked emission line profile (Sandage 1966; Lynds 1968). It is also an extended double-lobed FR II radio source. Leahy & Perley (1995) discussed the jets and hotspots of it and they also provided some basic data of this source. The VLBI observations at 5 GHz show evidence of superluminal motions, with $v/c \approx 4.0$ (Alef et al. 1996). 3C 390.3 has a well known history, both in the continuum light and in emission lines(e.g., Dietrich et al. 1998; Shapovalova et al. 2001; Sandage 1967, 1973; Zheng 1996). Prieto & Kotilainen(1997) detected optically-resolved emission coincident with the brightest region of the northern radio lobe (hot spot B) in B, R, and I bands. Dunn et al.(2006) provided a database of Ultraviolet continuum light curves for AGNs, and 3C 390.3 is one of them. *ROSAT PSPC* of 3C 390.3 show resolved X-ray emission spatially located at the position of the northern radio hotspot(Prieto 1997). It is also a highly variable X-ray source (Inda et al. 1994; Eracleous et al. 1996; Wozniak et al. 1998; Leighly et al. 1997; Leighly & O'Brien 1997; Gliozzi et al. 2003). Gaskell(2006) discussed the relationship between the X-ray, UV, and optical variability in 3C 390.3. The narrow-line region in 3C 390.3 is probably on the order of 1 lt yr, and a significant part of the NLR is located near the line of sight(Zheng et al. 1995). The black hole mass of 3C 390.3 has been estimated through reverberation mapping (e.g., McLure & Dunlop 2001; Botte et al. 2004; Shapovalova et al. 2001), ranging from 2.2×10^8 to $2.1 \times 2.1^9 M_{\odot}$.

3C 390.3 has been one of our primary targets for long-term monitoring in the optical band at the Shanghai Astronomical Observatory(SHAO). In this paper, we present V, R, and I data taken in the period from 1995 to 2004. We also compile historical data from 1894 to 2004. We obtain a total of 786 observational points, to which we adopt the *CLEANest* method to search for periodicities.

2. Observations and data reduction

The observations presented here were obtained with the 1.56-m telescope at SHAO from 1995 March 6 to 2004 August 14. At first a liquid nitrogen cooled CCD camera (1024×1024 pixels, 1 pixel = 0.019 mm) was used. The field of view of this was 4.3 arcminutes (1 pixel = 0.25 arcsec) when used directly at the Cassegrain focus, and approximately 13 arcmins (1 pixel = 0.76 arcsec) when used with a focal reducer. A new liquid nitrogen cooled CCD camera (2048×2048 pixels, SITe CCD chip) has been used since August, 2002. The chip of this camera subtends 11 arcmin by 11 arcmin in sky, with a scale is 0.31 arcsec per pixel (1 pixel = 0.024 mm). Standard Johnson-Cousins V, R, and I filters were used. Typical integration times were 300 s for I and R, and 600 s for filter V, depending on sky conditions

and the brightness of 3C 390.3. The flat field images were taken at dusk and dawn. The bias images were taken at the beginning and the end of the observations, while the dark-field images were taken at the end. All observing data were processed using the IRAF software package.

The seeing at the Sheshan Station of SHAO varied from 1.3 to 2.0 arcseconds FWHM and we have discussed this elsewhere (see Fig. 3 of Qian et al. 2002). Since 3C 390.3 is not a point-like source, seeing fluctuations may have an effect. Thus, we have followed the recommendations of Cellone et al. (2000) and selected a photometric aperture of radius 6.5 arcseconds to minimize potential seeing-dependent effects. Cellone et al. (2000) gave the minimum aperture radii in Table 2 of their paper, for a V=16 mag. AGN and various host galaxy for magnitudes V_G . The fainter the V_G , the smaller the photometric radii that can be used. Shapovalova et al. (2001) used a 10 arcsec diameter photometric aperture, corresponding a 5 arcsec radius aperture, which is also comparable to the one we have used. We used comparison stars A, B, and D of Penston et al. (1971) and HST GS 4951:731. V, R, and I magnitudes were taken from Dietrich et al. (1998). Using differential photometry with respect to each comparison star, $c_i, i = 1 - n$, within the frame we obtain a magnitude m_i for the object of interest. Then the object's magnitude at that time is

$$\bar{m} = \frac{\sum m_i}{n}, \quad (1)$$

where n is the number of standard stars, in this case, 4. The uncertainty σ_1 was calculated as

$$\sigma_1 = \sqrt{\frac{\sum (m_i - \bar{m})^2}{n - 1}}. \quad (2)$$

The difference between comparison stars is

$$\sigma_2 = (m_A - m_B) - \Delta m_{AB}, \quad (3)$$

where Δm_{AB} is the magnitude difference of comparison stars A and B as given by Dietrich et al. (1998), and m_A and m_B are the observed magnitudes of comparison stars A and B. The absolute value of σ_2 was used as an additional indicator of the observational uncertainty.

The observational data are listed in Tables 1–3, in which the first column gives the Julian date, the second column the magnitudes, the third the σ_1 uncertainties, and the fourth the σ_2 uncertainties.

3. The light curves

Figures 1 – 3 show the light curves of 3C 390.3 and the magnitude differences between comparison stars A and B in the V, R, and I filters, respectively. In our observation period

from March 1995 to August 2004, variations of $1^m.372(15.023 \text{ to } 16.395)$ in the V band, $1^m.240(14.352 \text{ to } 15.592)$ in the R band, and $1^m.284(13.896 \text{ to } 15.180)$ in the I band are found. The observations show that 3C 390.3 was brightening from 1995 and reached its brightest in 1996 September. Then it slowly declined in brightness, but was brightening again in September 2003.

We have compared our results with those of Dietrich et al.(1998). Our data have 10 days of overlap with the data of Dietrich et al. We converted their published flux data of 3C 390.3 to V magnitudes by taking $V = -2.5 \times \log(f) + 17.961$. For each day, the observational data were averaged and they were shown in Fig. 4. This comparison gave the relationship used to convert their fluxes to V magnitudes.

Dunn et al.(2006) determined the UV light curves of 3C 390.3 using the Multimission Archive at STScI. The data were observed with the International Ultraviolet Explorer, from 1978 to 1996. The light curves of the three bands, centered at 1431, 1816, and 1912 Angstroms, all show a brightening trend from JD 2449750 to JD 2450162, which is consistent with our V, R, and I light curves for the same period.

4. The Historical Light Curve and Possible Periodicities

4.1. Historic Light Curve

We have reconstructed the historical light curve by combining our recent data with data from the literature (Cannon et al. 1971; Selmes et al. 1975; Dietrich et al. 1998; Scott et al. 1976; Sergeev et al. 2002; Lloyd 1984; Shapovalova et al. 2001; Sandage 1967, 1973; Shen et al. 1972; Yee & Oke 1981; Pica et al. 1980, 1988). Most of these data set are for the V band or continuum near V band. However, there are some B band data in the remaining papers. In order to include these data, we needed to convert them to V band magnitude. Shapovalova et al. (2001) provide simultaneous B and V data (see Fig. 5). From their data we find that $V = 7.234 + 0.508B$ with a standard deviation of 0.052 mag. This relationship was then used to convert B-band magnitudes to V-band magnitudes to give a historical light curve in the V band. This has a total of 786 observational points over a time interval of 111 years (from 1894 to 2004). We show the historical light curve in Fig. 6. It shows two outbursts (1970 and 1996) and a possible third outburst (near 1939).

4.2. Periodicity Analysis

Using the historical light curve we have constructed for 3C 390.3, we searched for possible periodicities.

As in our previous papers, we use the *CLEANest* analysis (Foster 1995) to search for periodicities (Fan et al. 2006, 2007). The *CLEANest* analysis cleans spurious periodicities as follows. First, the strongest single peak and corresponding aliases are subtracted from the original spectrum, then the residual spectrum is scanned to determine whether the next strongest remaining peak is statistically significant. If so, then the original data are analyzed to find the pair of frequencies which best models the data, these two peaks and corresponding aliases are subtracted, and the residual spectrum is scanned again. The process continues, producing successive *CLEANest* spectra, until all statistically significant frequencies are included.

The light curve of 3C 390.3 shows that the data are unevenly sampled with most data concentrated in the period from 1965 to 2004. Observations before 1933 are particularly sparse. After using the *CLEANest* algorithm on the 1933–2004 data set we find that there are seven independent frequency components required to “clean” the light curve. The *CLEANest* spectrum is shown in Fig. 7. For comparison, in Fig. 10 we show the results of using only the post 1965 data.

When analyzing unevenly sampled time series, the irregular spacing introduces many complications into the Fourier transformations; it can alter peak frequencies (slightly) and amplitudes (greatly), and even introduce extremely large spurious peaks. Including all 3C 390.3 data points would not only give irregular sampling but would also give undue weight to the most recent 40 yr of data. To obtain regular sampling and to give more uniform weighting to different epochs we binned the data from 1933 onwards. However, binning data inevitably throws away information. To minimize this we adopted a bin size of 0.02 yr (7.30 days) which is short enough compared to the long-term periods we are looking for (years) and thus unlikely to distort long-term variations. This binning gives us 361 points in the binned light curve from 1933 to 2004. In Fig. 8 we show the *CLEANest* spectrum for this binned light curve.

We also investigated the effect of removing a long-term linear trend in the binned 1933–2004 historical light curve using $V(\text{magnitude}) = -0.849005 + 0.00820992 \times t(\text{year})$. In Fig. 9 we show the *CLEANest* spectrum for this light curve.

Following Foster(1996), the variance of a frequency $\text{Var}(\omega)$ and the variance of the

amplitude of the given frequency $Var(P)$ can be estimated by:

$$Var(\omega) = \frac{24\sigma_{res}^2}{NA^2T^2} \quad (4)$$

$$Var(P) = \frac{2\sigma_{res}^2}{N} \quad (5)$$

where σ_{res} is the variance of the residual data, A is the amplitude of the given frequency and T is the total time span, and N means the number of data values in an observed time series. The σ_{res}^2 is estimated by

$$\sigma_{res}^2 = \frac{NV_{res}}{N - 3f - 1}, \quad (6)$$

where V_{res} is the variance of residual data, $V_{res} = \langle res|res \rangle - \langle 1|res \rangle$, and f is the number of discrete frequencies. $|x\rangle$ represent a vector in a N -dimensional vector space.

$$|x\rangle = [x(t_1), x(t_2), \dots, x(t_N)] \quad (7)$$

Defining the inner product of two vectors, $|f\rangle$ and $|g\rangle$, as the average value of the product fg over the sampling t_α

$$\langle f|g \rangle = \frac{\sum_{\alpha=1}^N f(t_\alpha)g(t_\alpha)}{N} \quad (8)$$

Defining the constant vector $|1\rangle$ as

$$|1\rangle = [1, 1, \dots, 1]. \quad (9)$$

The variation of a vector $|f\rangle$ is

$$V_f = \langle f|f \rangle - \langle 1|f \rangle^2 \quad (10)$$

The results of these four *CLEANest* analyses are listed in Table 4. In this table we also give the False Alarm Probability (FAP) of each of the *CLEANest* frequency components, which depends on the amplitude. Small FAP values support the reality of these periodicities (see Fan et al. 2006 for details).

The unbinned V-band data, the binned data, the linear-trend removed data, and the post-1965 data (see Table 4) all show that there are apparent periodicities. Those matched periods derived from the first three data sets are: 13298 ± 6298 days(15268 ± 10857 days), 3700 ± 413 days (3296 ± 387 days, 3026 ± 427 days), 1871 ± 106 days (1759 ± 110 days, 1961 ± 179 days), 1297 ± 51 days(1282 ± 77 days), and 775 ± 18 days (775 ± 21 days, 776 ± 28 days). However, since the period 13298 ± 6298 days(15268 ± 10857 days) is almost

the length of the data coverage, the period is not a physically significant one. From Fig. 6, we can see that most data was sampled in the period of 1965 to 2004(about 40 years). Therefore, we reinvestigated periods based on the post 1965 data. The matched periods derived from the V band data(1933-2004) and the post 1965 data(1965-2004) are: 7022 ± 1486 days(7203 ± 1564 days), 3700 ± 413 days(3660 ± 404 days), 1297 ± 51 days(1306 ± 51 days), 847 ± 22 days(847 ± 22 days), and 238 ± 2 days(238 ± 2 days). In Table 4, we also present the phase of the corresponding period. Phase and period can be used to identify a signal in multi-data set. We used the obtained components to fit all the light curves and the results are shown in Fig. 11.

According to the data processing theory, the results derived from the linear-trend removed data set is more reliable. So the possible periods are: 8.30 ± 1.17 , 5.37 ± 0.49 , 3.51 ± 0.21 , and 2.13 ± 0.08 years.

5. Discussion and Conclusions

AGNs are variable throughout the whole electromagnetic spectrum. In our monitoring program, we have observed the galaxy 3C 390.3 from March 1995 to August 2004. The observations clearly show that the source is variable in the optical band with the variation amplitude of $1^m.372$, $1^m.240$, and $1^m.284$ in the V, R, and I bands respectively. The V band historical light curve is compiled, which has a time span of 111 years. Possible periods of 8.30 ± 1.17 , 5.37 ± 0.49 , 3.51 ± 0.21 , and 2.13 ± 0.08 years were found in the light curve by means of *CLEANest* method.

It has been suggested that the long-term periodic outbursts of OJ 287 may be explained by a binary black hole (Sillanpää et al. 1988) or such outbursts may be due to thermal and viscous instabilities in a thin accretion disk (Meyer & Meyer-Hofmeister 1984; Horiuchi & Kato 1990). The historical light curve of 3C 390.3 shows strong variability. Several possible periods were found by *CLEANest* method. The multiple periods we derived may imply the instabilities in the disk. The analysis of spectra of 3C 390.3 covering a period of over 20 yr may indicate the binary black hole model(Gaskell 1996). Shapovalova et al.(2001) have monitored this object between 1995 and 2000. Their results do not support either the models of outflowing biconical gas streams or those of supermassive binary black holes. They conclude that they favor the accretion disk model.

This work is partially supported by the Joint Laboratory for Optical Astronomy of Chinese Academy of Sciences, the National Natural Science Foundation of China (10573005,10633010), the 973 project (No. 2007CB815405), and Science & Technology Commission of Shanghai

Municipality (06DZ22101). We thank Martin Gaskell for editing the English and for comments. We are grateful to the referee, Dr. Paul Viita for his valuable comments.

REFERENCES

- Alef, W., et al. 1996, A&A, 308, 376
Botte, V., et al. 2004, AJ, 127, 3168
Cannon, D. R., et al. 1971, MNRAS, 152, 79
Cellone, S. A., Romero, G. E., & Combi, J. A. 2000, AJ, 119, 1534
Dietrich, M., et al. 1998, ApJS, 115, 185
Dunn, J. P., et al. 2006, PASP, 118, 572
Eracleous, M., et al. 1996, ApJ, 459, 89
Fan, J.H., Liu, Y., Yuan, Y.H., et al. 2007, A&A, 462, 547
Fan, J.H., Liu, Y., Yuan, Y.H., et al. 2006, PASJ, 58, 797
Fan, J. H., 2005, ChJA&A Suppl., 5, 213
Fan, J. H., Lin R. G., Xie, G. Z., et al. 2002, A&A, 381, 1
Fan, J.H., 1999, MNRAS, 308, 1032
Fan, J. H., Xie, G. Z., Lin, R.G., et al. 1997, A&AS, 125, 525
Foster, G. 1996, AJ, 111, 541
Foster, G. 1995, AJ, 109, 1889
Gaskell, C. M. 1996, ApJ, 464, L107
Gaskell, C. M. 2006, ASP Conf. Ser., 360, 111
Gliozzi, M., Sambruna, R., & Eracleous, M. 2003, ApJ, 584, 176
Horiuchi, T., & Kato, S. 1990, PASJ, 42, 661
Inda, M., et al. 1994, ApJ, 420, 143

- Jurkevich, I., Usher, P. D., & Shen, B. S. P. 1971, *Ap&SS*, 10, 402
- Kidger, M., Takalo, L., & Sillanpää, A. 1992, *A&A*, 264, 32
- Lainela, M., et al. 1999, *ApJ*, 521, 561
- Leahy, J. P., & Perley, R. A. 1995, *MNRAS*, 277, 1097
- Leighly, K. M., et al. 1997, *ApJ*, 483, 767
- Leighly, K. M., & O'Brien, P. T. 1997, *ApJ*, 481, L15
- Liller, M. H. & Liller, W. 1975, *ApJ*, 199, L133
- Lloyd, C. 1984, *MNRAS*, 209, 697
- Lynds, C. 1968, *AJ*, 73, 888
- McLure, R. J., & Dunlop, J. S. 2001, *MNRAS*, 327, 199
- Meyer, F., & Meyer-Hofmeister, E. 1984, *A&A*, 132, 143
- Miller, H. R. 1975, *ApJ*, 201, L109
- Osterbrock, D. E., Koski, A. T., & Phillips, M. M. 1975, *ApJ*, 197, L41
- Penston, M. J., Penston, M. V., & Sandage, A. R. 1971, *PASP*, 83, 783
- Pica, A. J., et al. 1980, *AJ*, 85, 1442
- Pica, A. J., et al. 1988, *AJ*, 96, 1215
- Pollock, J. T. 1975, *ApJ*, 198, L53
- Prieto, M. A. 1997, *MNRAS*, 284, 627
- Prieto, M. A., & Kotilainen, J. K. 1997, *ApJ*, 491, L77
- Qian, B. C., & Tao, J. 2004, *PASP*, 116, 161
- Qian, B. C., Tao, J., & Fan, J. H. 2002, *AJ*, 123, 678
- Sandage, A. 1966, *ApJ*, 145, 1
- Sandage, A. 1967, *ApJ*, 150, L177
- Sandage, A. 1973, *ApJ*, 180, 687

- Scott, R. L., et al. 1976, AJ, 81, 7
- Selmes, R. A., et al. 1975, MNRAS, 170, 15
- Sergeev, S. G., et al. 2002, ApJ, 576, 660
- Shapovalova, A. I., et al. 2001, A&A, 376, 775
- Shen, B. S. P., et al. 1972, ApJ, 171, 457
- Sillanpää, A., Haarala, S., Valtonen, M. J., Sundelius, B., & Byrd, G. G. 1988, ApJ, 325, 628
- Tao, J., Qian, B. C., & Fan, J. H. 2004, PASP, 116, 634
- Wozniak, P. R., et al. 1998, MNRAS, 299, 499
- Yee, H. K. C., & Oke, J. B. 1981, ApJ, 248, 472
- Zheng, W. 1996, AJ, 111, 1498
- Zheng, W., Perez, E., Grandi, S. A., & Penston, M. V. 1995, AJ, 109, 2355

Table 1. V-band magnitudes of 3C 390.3

Date(JD - 2449000)	Magnitude	σ_1	σ_2
783.3201	15.658	0.010	-0.004
783.3259	15.503	0.014	-0.016
783.3349	15.589	0.010	0.004
802.3073	15.696	0.023	-0.055
802.3107	15.450	0.014	0.003
803.3255	15.576	0.028	-0.055
845.1668	15.383	0.007	0.001
845.1734	15.594	0.004	0.000
924.0950	15.513	0.026	0.041
924.1245	15.598	0.019	0.028
935.0480	15.585	0.038	-0.051
935.0582	15.539	0.013	-0.001
935.0627	15.492	0.028	-0.040
943.0259	15.470	0.015	-0.025
943.0345	15.461	0.025	-0.047
947.0802	15.330	0.025	0.049
947.0870	15.436	0.025	0.049
977.9790	15.310	0.024	0.043
977.9976	15.320	0.043	0.087
978.0020	15.322	0.053	0.072
1196.2712	15.114	0.093	0.031
1196.2934	15.332	0.032	0.047
1197.2786	15.303	0.048	-0.053
1197.2850	15.480	0.041	-0.001
1199.2778	15.445	0.036	0.032
1199.2833	15.146	0.008	0.012
1221.1243	15.050	0.035	-0.047
1257.0869	15.328	0.044	-0.023
1257.0953	15.157	0.063	0.053
1328.0242	15.119	0.053	-0.075
1328.0316	15.382	0.047	0.047

Table 1—Continued

Date(JD - 2449000)	Magnitude	σ_1	σ_2
1328.0402	15.047	0.073	-0.020
1334.0357	15.046	0.040	-0.014
1334.0427	15.056	0.035	-0.048
1371.9932	15.681	0.043	0.024
1372.0024	15.367	0.081	0.060
1550.3632	15.498	0.038	0.081
1577.2818	15.386	0.018	-0.040
1577.2894	15.408	0.041	-0.072
1577.2964	15.521	0.040	-0.081
1577.3030	15.579	0.041	-0.068
1586.2854	15.883	0.009	0.001
1586.3046	15.602	0.021	-0.005
1594.2563	15.361	0.059	-0.073
1594.2604	15.388	0.029	0.055
1594.2646	15.645	0.026	-0.052
1599.1615	15.570	0.017	0.019
1614.2056	15.515	0.035	-0.080
1614.2110	15.591	0.032	0.057
1614.2210	15.427	0.098	-0.034
1616.1638	15.764	0.027	-0.002
1616.1776	15.810	0.031	-0.015
1660.1593	15.590	0.074	-0.077
1660.1655	15.823	0.053	0.095
1692.0016	15.633	0.030	-0.017
1692.0042	15.741	0.024	-0.031
1692.0264	15.562	0.035	-0.061
1692.0333	15.432	0.024	0.019
1701.0160	15.731	0.024	-0.032
1701.0196	15.945	0.019	-0.011
2229.3530	15.518	0.027	0.004
2318.3192	15.853	0.045	-0.003

Table 1—Continued

Date(JD - 2449000)	Magnitude	σ_1	σ_2
2348.1668	16.380	0.090	0.087
2348.1746	16.260	0.081	0.010
2437.0529	16.395	0.078	0.110
3041.2721	15.430	0.083	-0.118
3041.2866	15.673	0.087	-0.124
3094.2237	15.272	0.065	0.092
3094.2386	15.306	0.103	0.054
3100.1232	15.489	0.042	0.001
3112.3400	15.581	0.093	0.132
3518.0847	15.888	0.069	-0.023
3856.0297	15.242	0.063	-0.045
3856.0446	15.170	0.059	-0.083
3888.0554	15.023	0.068	0.096
3888.0695	15.733	0.069	0.097
4231.7777	16.060	0.060	-0.063

Table 2. R-band magnitudes of 3C 390.3

Date(JD - 2449000)	Magnitude	σ_1	σ_2
802.2993	15.206	0.052	0.073
802.3039	15.322	0.038	-0.025
803.3159	15.270	0.018	-0.003
819.0507	15.265	0.015	0.034
824.1183	15.234	0.040	0.049
845.1945	15.111	0.014	0.019
919.0410	15.305	0.028	0.052
924.0838	15.288	0.022	0.027
935.0480	15.149	0.015	0.027
943.0036	15.099	0.014	-0.005
943.0098	15.098	0.014	-0.004
947.0513	15.191	0.037	0.032
947.0587	15.154	0.035	0.066
977.9743	15.027	0.003	-0.004
977.9790	15.033	0.007	-0.010
977.9834	15.023	0.020	0.013
1196.2656	14.660	0.021	0.021
1196.2876	14.608	0.040	0.021
1197.2695	14.698	0.019	0.003
1197.2740	14.661	0.024	-0.029
1199.2660	14.820	0.035	0.041
1199.2722	14.775	0.044	0.056
1221.0993	14.769	0.024	0.035
1257.0738	14.880	0.054	0.034
1257.0799	14.871	0.045	-0.052
1328.0826	14.352	0.019	0.028
1328.0873	14.402	0.082	0.048
1328.0929	14.504	0.060	0.003
1332.0358	14.944	0.067	-0.095
1371.9859	14.656	0.062	0.030
1371.9889	14.718	0.086	0.031

Table 2—Continued

Date(JD - 2449000)	Magnitude	σ_1	σ_2
1550.3524	15.144	0.012	-0.027
1550.3569	15.083	0.020	0.028
1577.3114	15.083	0.045	0.056
1577.3167	15.029	0.039	0.061
1577.3217	15.078	0.034	0.052
1577.3267	14.978	0.040	0.059
1577.3330	14.990	0.039	0.062
1586.2576	14.828	0.046	0.069
1586.2617	15.274	0.032	0.038
1586.2704	15.169	0.020	0.007
1586.2747	15.171	0.023	0.022
1586.2793	15.213	0.042	0.069
1594.2340	15.122	0.042	0.065
1594.2422	14.994	0.024	-0.012
1594.2447	15.196	0.024	0.019
1599.1528	15.192	0.047	0.060
1614.2360	15.219	0.015	0.019
1614.2418	15.191	0.016	0.016
1616.1541	15.138	0.020	0.029
1616.1572	15.211	0.015	0.021
1616.1600	15.271	0.030	0.056
1660.1492	15.339	0.034	0.008
1660.1524	15.210	0.021	0.012
1691.9937	15.205	0.014	-0.015
1691.9959	15.198	0.012	0.020
1691.9981	15.217	0.018	-0.005
1692.0182	15.181	0.014	0.027
1692.0209	15.170	0.027	0.032
1692.0234	15.223	0.030	0.005
1699.1292	15.067	0.029	0.009
1699.1339	15.181	0.034	0.045

Table 2—Continued

Date(JD - 2449000)	Magnitude	σ_1	σ_2
1701.0020	15.317	0.029	0.024
1701.0053	15.301	0.007	0.013
1701.0087	15.373	0.006	0.003
1701.0122	15.380	0.029	-0.042
2229.3450	15.099	0.034	0.018
2318.3073	14.846	0.034	0.049
2348.1569	15.211	0.037	0.053
2348.1621	15.198	0.044	0.062
2437.0420	15.273	0.049	0.070
2757.3133	15.010	0.057	0.080
3017.2940	14.905	0.045	-0.051
3017.3345	15.014	0.049	-0.070
3018.3446	14.897	0.035	-0.049
3041.2560	14.911	0.071	0.062
3041.2636	14.955	0.038	0.078
3091.1142	14.839	0.087	0.022
3091.1253	15.106	0.066	0.076
3093.2495	14.950	0.057	0.026
3094.2063	14.977	0.036	0.027
3094.2139	14.991	0.052	-0.024
3100.1131	15.085	0.082	-0.023
3108.1328	15.135	0.071	-0.078
3108.1425	15.108	0.005	0.002
3112.3128	15.127	0.063	-0.040
3124.1414	15.023	0.021	0.012
3124.1552	15.033	0.079	0.010
3518.0390	15.211	0.119	0.168
3518.0766	15.329	0.099	-0.140
3519.0071	14.841	0.047	0.066
3519.0510	14.828	0.068	0.096
3856.0247	15.130	0.016	0.023

Table 2—Continued

Date(JD - 2449000)	Magnitude	σ_1	σ_2
3856.0399	15.000	0.028	0.040
3873.9964	15.075	0.052	0.074
3887.9728	14.451	0.069	-0.098
3887.9856	15.090	0.144	-0.204
3887.9983	14.409	0.053	0.045
3888.0113	14.985	0.052	0.074
4231.7682	15.592	0.098	-0.139

Table 3. I-band magnitudes of 3C 390.3

Date(JD 2449000+)	Magnitude	σ_1	σ_2
783.3399	14.635	0.019	-0.036
783.3429	14.627	0.028	-0.008
783.3463	14.719	0.021	-0.038
783.3556	14.696	0.022	-0.044
802.3145	14.470	0.014	0.002
803.3013	14.600	0.019	-0.029
803.3078	14.551	0.019	-0.023
845.2020	14.532	0.023	0.004
845.2187	14.575	0.028	0.017
845.2234	14.566	0.030	0.030
919.0351	14.645	0.041	0.023
919.0451	14.629	0.038	-0.031
924.0796	14.630	0.045	-0.025
924.1049	14.690	0.056	0.020
934.9925	14.567	0.028	-0.043
935.0350	14.505	0.040	-0.076
935.0395	14.491	0.041	-0.036
942.9844	14.568	0.022	-0.018
942.9920	14.536	0.015	-0.017
947.0385	14.547	0.065	-0.001
947.0445	14.623	0.066	-0.001
961.9682	14.409	0.035	-0.017
961.9741	14.452	0.054	-0.032
961.9825	14.431	0.037	-0.012
977.9529	14.374	0.041	0.003
977.9578	14.432	0.039	-0.032
977.9626	14.389	0.092	-0.184
1196.2602	14.105	0.023	-0.013
1196.2785	14.096	0.039	-0.092
1197.2588	14.081	0.033	0.036
1197.2646	14.223	0.032	0.044

Table 3—Continued

Date(JD 2449000+)	Magnitude	σ_1	σ_2
1199.2347	14.287	0.016	-0.004
1199.2490	14.219	0.025	0.000
1199.2556	14.220	0.022	-0.026
1221.0931	14.098	0.028	0.034
1257.0579	14.292	0.019	-0.007
1257.0645	14.238	0.031	0.004
1371.9801	14.117	0.028	-0.042
1550.3434	14.394	0.018	0.026
1550.3469	14.346	0.037	0.053
1577.2501	14.452	0.009	0.004
1577.2542	14.439	0.022	0.026
1577.2606	14.537	0.024	0.004
1577.2678	14.491	0.024	-0.012
1577.2715	14.469	0.025	0.013
1578.2352	14.378	0.040	0.035
1578.2389	14.553	0.065	0.096
1578.2842	14.512	0.047	0.019
1578.2877	14.503	0.069	0.075
1586.3170	14.578	0.014	-0.021
1586.3204	14.586	0.025	0.016
1586.3255	14.575	0.027	0.035
1594.2498	14.530	0.030	0.041
1594.2519	14.508	0.021	0.011
1594.2536	14.519	0.036	0.040
1599.1410	14.556	0.040	0.039
1599.1462	14.559	0.030	0.048
1614.1925	14.625	0.040	-0.085
1614.1991	14.602	0.031	-0.065
1614.2020	14.578	0.032	-0.062
1616.1458	14.620	0.013	0.011
1616.1483	14.536	0.092	0.015

Table 3—Continued

Date(JD 2449000+)	Magnitude	σ_1	σ_2
1616.1509	14.528	0.091	0.033
1660.1375	14.905	0.041	-0.027
1660.1424	14.353	0.060	0.011
1660.1455	14.488	0.027	-0.013
1691.9837	14.575	0.028	-0.058
1691.9864	14.474	0.020	-0.007
1691.9895	14.543	0.033	-0.073
1692.0115	14.525	0.042	0.034
1692.0139	14.425	0.021	0.030
1692.0157	14.386	0.015	-0.006
1699.1103	14.432	0.009	0.009
1699.1143	14.562	0.013	0.017
1699.1182	14.510	0.013	0.009
1699.1234	14.268	0.035	-0.070
1700.9910	14.760	0.004	0.007
1700.9941	14.630	0.014	-0.027
1700.9972	14.784	0.035	-0.055
1700.9992	14.838	0.015	-0.010
2088.9659	14.368	0.029	-0.051
2229.3354	14.606	0.011	0.000
2229.3390	14.587	0.003	0.001
2318.2813	14.472	0.038	0.037
2318.2947	14.514	0.049	0.028
2348.1474	14.723	0.023	0.012
2348.1517	14.712	0.025	0.035
2437.0209	14.834	0.033	0.024
2437.0278	14.679	0.008	0.012
2437.0355	14.697	0.074	0.066
2633.3729	14.730	0.057	-0.088
2696.0850	14.778	0.100	-0.018
2696.1289	14.946	0.004	-0.006

Table 3—Continued

Date(JD 2449000+)	Magnitude	σ_1	σ_2
2701.2598	14.527	0.013	-0.018
2701.2719	14.586	0.019	0.006
2701.3009	14.572	0.028	-0.052
2702.2897	14.803	0.017	-0.015
2708.2299	14.678	0.039	-0.029
2708.2428	14.420	0.034	-0.048
2708.2686	14.429	0.082	0.035
2708.2820	14.356	0.020	-0.029
2741.2177	14.580	0.078	0.019
2742.0505	14.651	0.048	-0.068
2742.0943	14.646	0.070	-0.099
2743.0436	14.595	0.030	-0.006
2743.0924	14.711	0.081	-0.019
2743.1037	14.457	0.094	-0.022
2746.0535	14.469	0.062	0.049
2746.0703	14.712	0.069	-0.092
2747.2671	14.472	0.046	-0.024
2752.2818	14.398	0.056	-0.010
2752.3235	14.309	0.055	0.066
2752.3354	14.496	0.074	-0.041
2757.2584	14.241	0.027	-0.038
2757.2833	14.270	0.006	-0.009
3017.2877	14.378	0.104	0.147
3017.3431	14.387	0.053	0.042
3018.3268	14.355	0.090	-0.036
3041.2464	14.469	0.024	-0.016
3041.2504	14.440	0.013	0.019
3091.1076	14.415	0.036	0.053
3091.1077	14.458	0.029	0.041
3091.1006	14.385	0.055	0.070
3091.1077	14.537	0.045	0.011

Table 3—Continued

Date(JD 2449000+)	Magnitude	σ_1	σ_2
3093.2401	14.535	0.012	0.000
3094.1951	14.413	0.027	0.049
3094.1994	14.440	0.035	0.024
3100.1083	14.745	0.028	-0.054
3108.1097	14.459	0.098	-0.081
3108.1206	14.575	0.064	-0.013
3112.3084	14.416	0.065	0.004
3124.1235	14.515	0.056	-0.041
3124.1323	14.510	0.039	-0.042
3760.2646	14.261	0.013	0.025
3760.2955	14.570	0.042	0.060
3795.2234	13.896	0.047	-0.067
3795.2569	13.978	0.074	-0.104
3855.1142	14.204	0.008	0.012
3855.1228	14.499	0.068	0.097
3856.0373	14.568	0.063	-0.089
3856.0520	14.471	0.085	-0.121
3857.0662	14.425	0.000	0.000
3874.9808	14.190	0.039	-0.055
3886.0060	14.286	0.188	-0.267
3886.0105	14.106	0.016	-0.022
3886.0435	14.180	0.060	-0.085
3887.9957	14.200	0.066	0.094
3888.0086	14.187	0.127	-0.180
3888.0216	13.987	0.078	0.110
4231.7819	15.106	0.021	0.030
4231.8011	15.180	0.042	-0.059

Period (d)	Amplitude	Phase (πrad)	FAP
V band data (1933–2004)			
7022 ± 1486	0.676 ± 0.083	−0.81 ± 0.12	0.002
3700 ± 413	0.325 ± 0.083	−1.00 ± 0.26	0.005
1871 ± 106	0.195 ± 0.083	0.92 ± 0.43	0.006
1297 ± 51	0.218 ± 0.083	0.40 ± 0.38	0.006
847 ± 22	0.321 ± 0.083	−0.13 ± 0.26	0.005
775 ± 18	0.315 ± 0.083	0.73 ± 0.26	0.005
239 ± 2	0.154 ± 0.083	−0.99 ± 0.54	0.007
Binned V band data (1933–2004)			
13298 ± 6298	0.648 ± 0.109	−0.79 ± 0.17	0.003
8738 ± 2720	0.598 ± 0.109	0.41 ± 0.18	0.003
3296 ± 387	0.187 ± 0.109	−0.69 ± 0.58	0.008
1759 ± 110	0.283 ± 0.109	−0.70 ± 0.38	0.006
947 ± 32	0.240 ± 0.109	0.86 ± 0.45	0.006
775 ± 21	0.313 ± 0.109	0.93 ± 0.40	0.005
233 ± 2	0.149 ± 0.109	0.21 ± 0.58	0.009
V band data (1933–2004) with linear-trend removed			
15268 ± 10857	0.687 ± 0.109	−0.52 ± 0.16	0.002
3026 ± 427	0.218 ± 0.109	−0.95 ± 0.50	0.007
1961 ± 179	0.224 ± 0.109	−0.26 ± 0.49	0.007
1282 ± 77	0.276 ± 0.109	0.11 ± 0.40	0.006
1169 ± 64	0.188 ± 0.109	0.00 ± 0.58	0.007
776 ± 28	0.273 ± 0.109	−0.11 ± 0.40	0.006
642 ± 19	0.207 ± 0.109	−0.57 ± 0.53	0.007
Post-1965 V band data			
7203 ± 1564	0.758 ± 0.082	−0.19 ± 0.11	0.002
3660 ± 404	0.347 ± 0.082	−0.59 ± 0.24	0.004
1306 ± 51	0.253 ± 0.082	0.06 ± 0.33	0.005
928 ± 26	0.342 ± 0.082	−0.91 ± 0.24	0.004
847 ± 22	0.332 ± 0.082	−0.67 ± 0.25	0.004
573 ± 10	0.137 ± 0.082	−0.11 ± 0.61	0.008
238 ± 2	0.127 ± 0.082	−0.61 ± 0.66	0.008

Table 4: Periodic components given by the *CLEANest* algorithm.

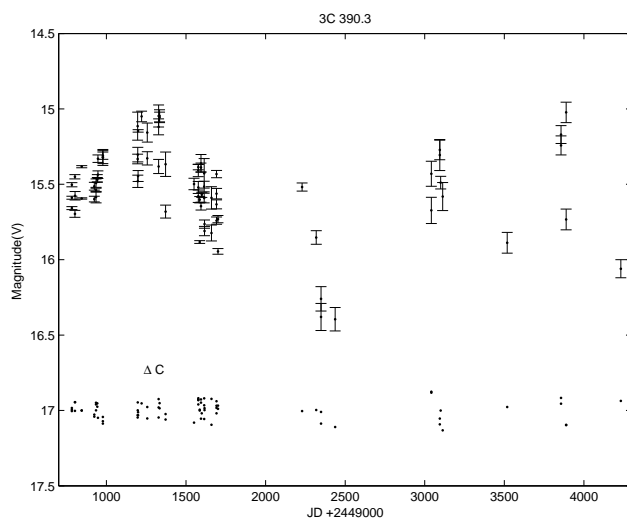


Fig. 1.— V-band light curve of 3C 390.3 (top) with the relative difference between comparison stars A and B (bottom).

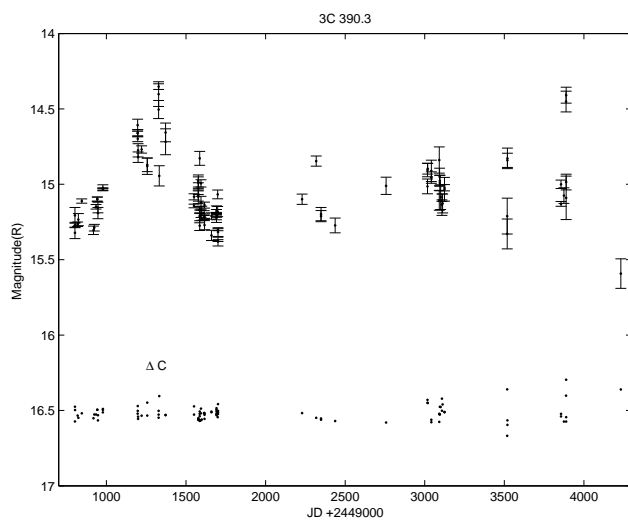


Fig. 2.— R-band Light curve of 3C 390.3 (top) with the relative differences between comparison stars A and B (bottom).

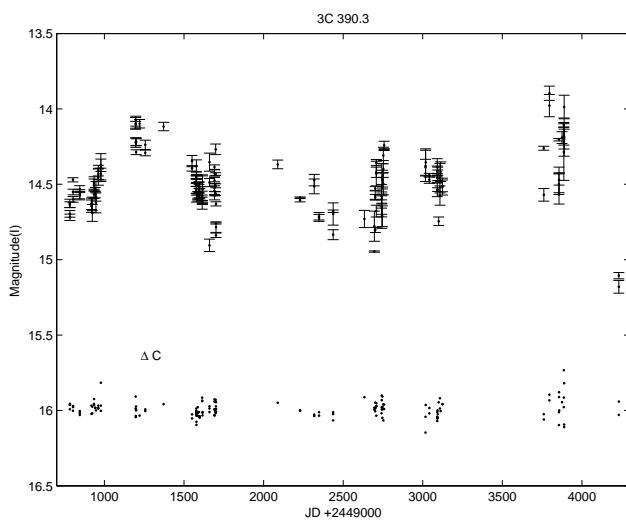


Fig. 3.— I-band light curve of 3C 390.3 (top) with the relative differences between comparison stars A and B (bottom).

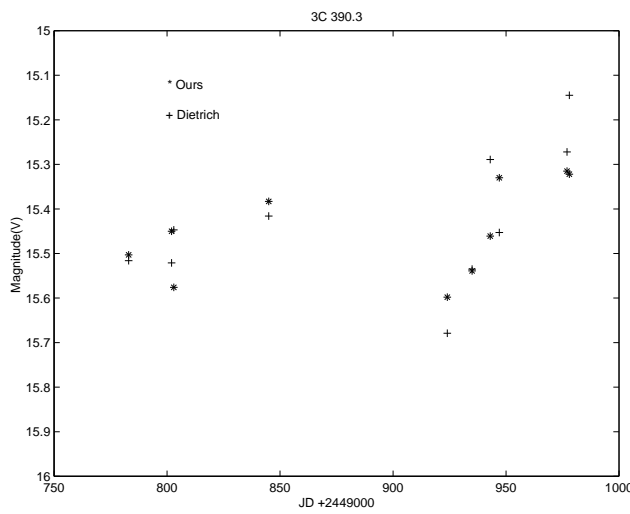


Fig. 4.— Comparison of the flux data given by Dietrich et al.(1998) with our V band data. The Dietrich et al. fluxes have been converted to magnitudes using the relationship $V = -2.5 \times \log(f) + 17.961$.

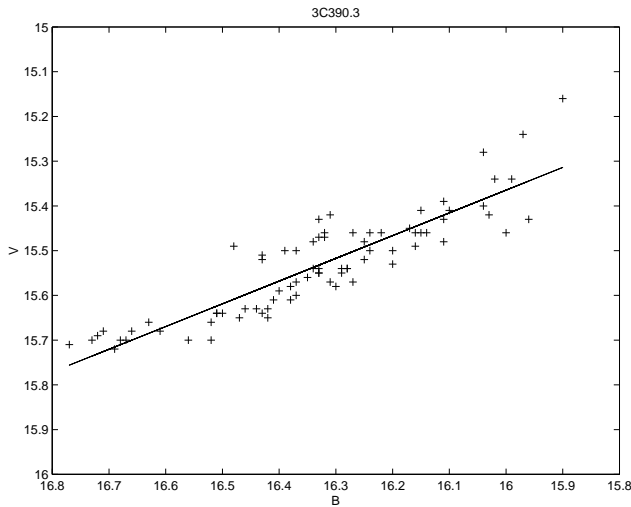


Fig. 5.— Comparison of B and V magnitudes given by Shapovalova et al. (2001).

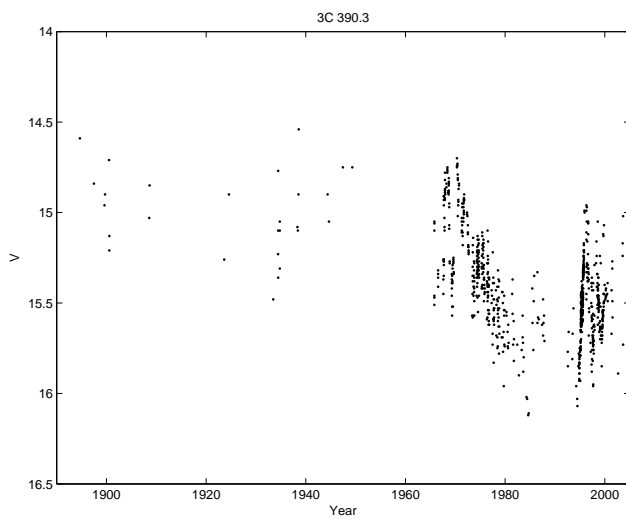


Fig. 6.— Reconstructed V-band historical light curve of 3C 390.3.

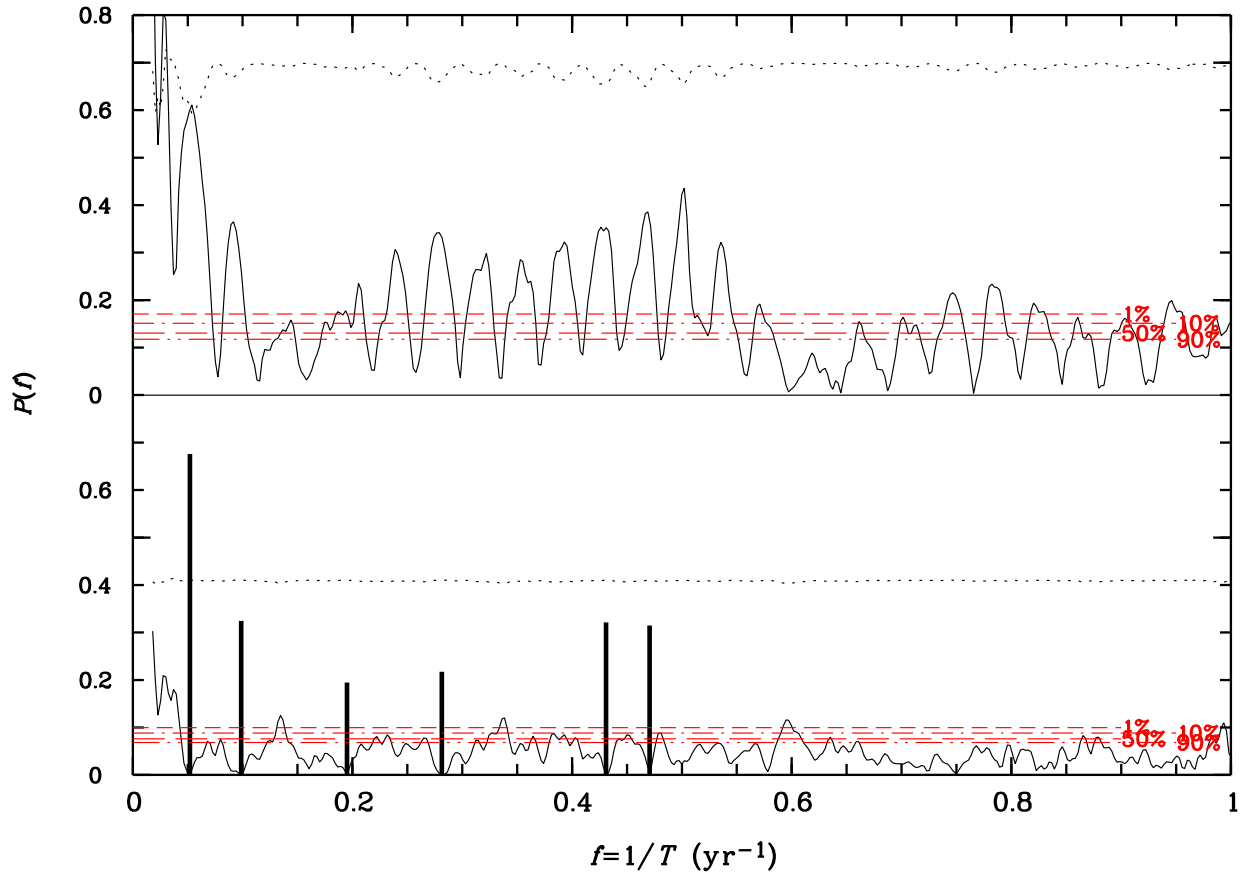


Fig. 7.— The Fourier power spectrum (top) and the *CLEANest* spectrum (bottom) for the V-band light curve of 3C 390.2 from 1933-2004. The dotted curves are the square deviations as a function of frequency. In the *CLEANest* spectrum, six *CLEANest* frequency components (thick vertical lines) and the residual spectrum are shown, one *CLEANest* component with a frequency of 1.53 yr^{-1} and an amplitude of 0.154 is off the figure. FAP significance levels of (from top to bottom) 0.01, 0.10, 0.50, 0.90 are marked.

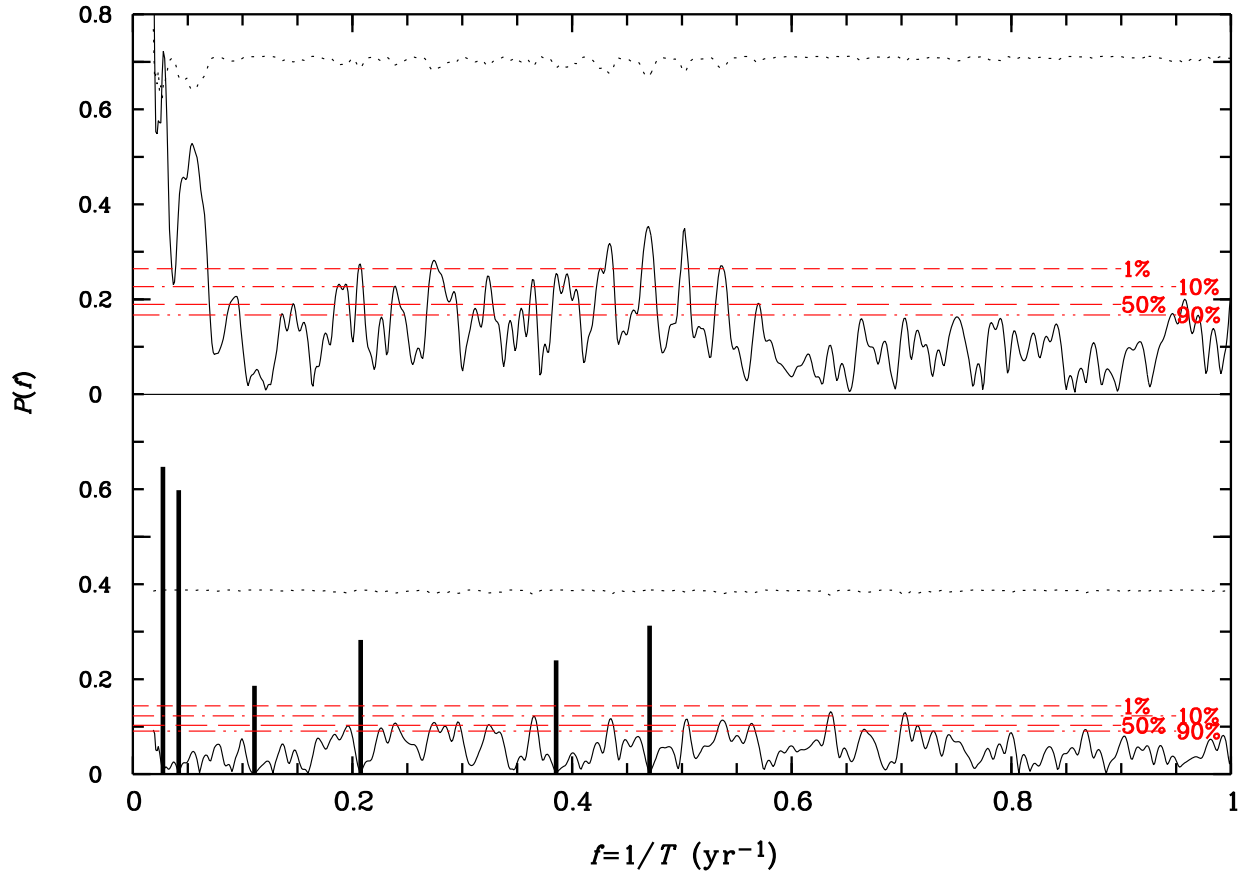


Fig. 8.— As for Fig. 7 but for the binned V-band light curve from 1933 to 2004. In the *CLEANest* spectrum, six *CLEANest* frequency components (thick vertical lines) and the residual spectrum are shown, one *CLEANest* component with a frequency of 1.57 yr^{-1} , and an amplitude of 0.149 is off the figure.

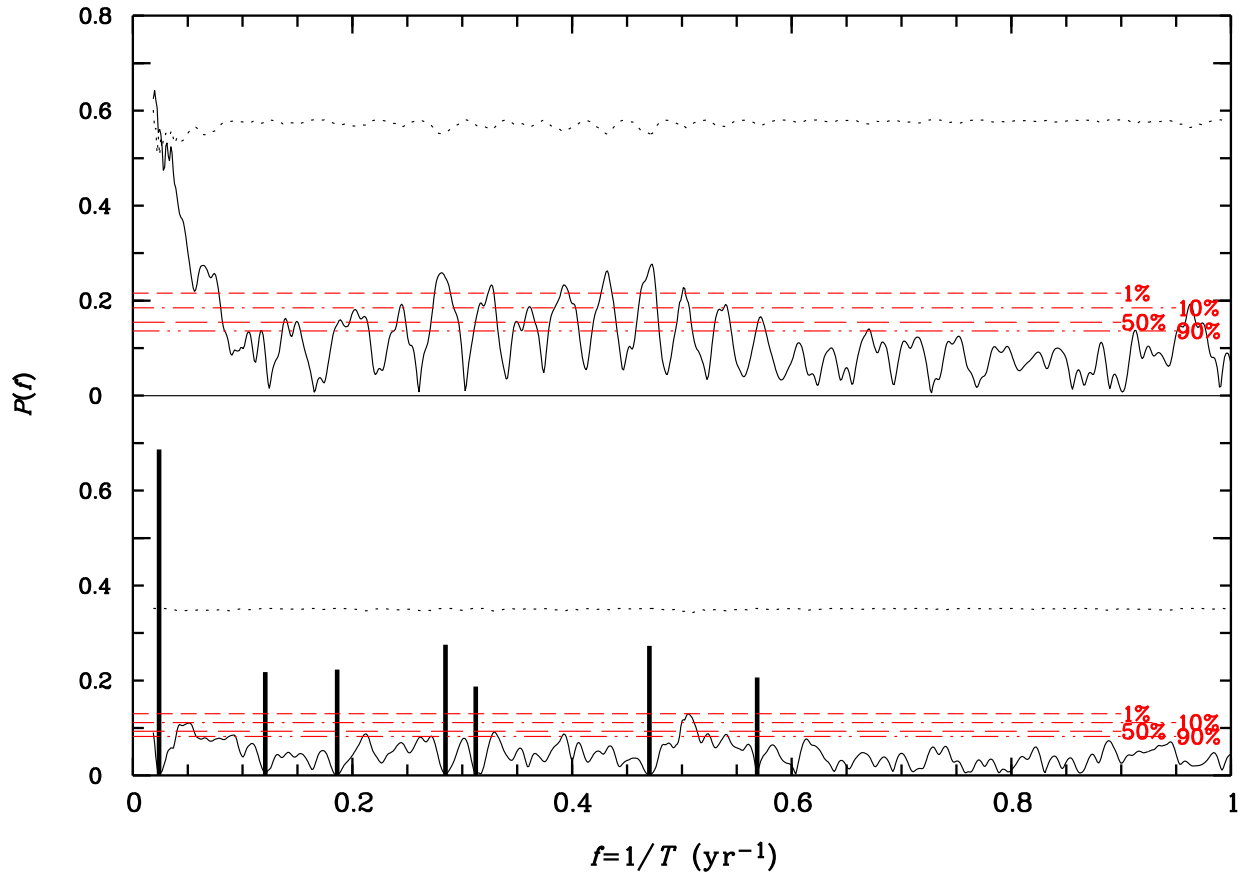


Fig. 9.— As for Fig. 7 but with a linear-trend removed from the light curve (see text). In the *CLEANest* spectrum, seven *CLEANest* frequency components are shown by thick vertical lines.

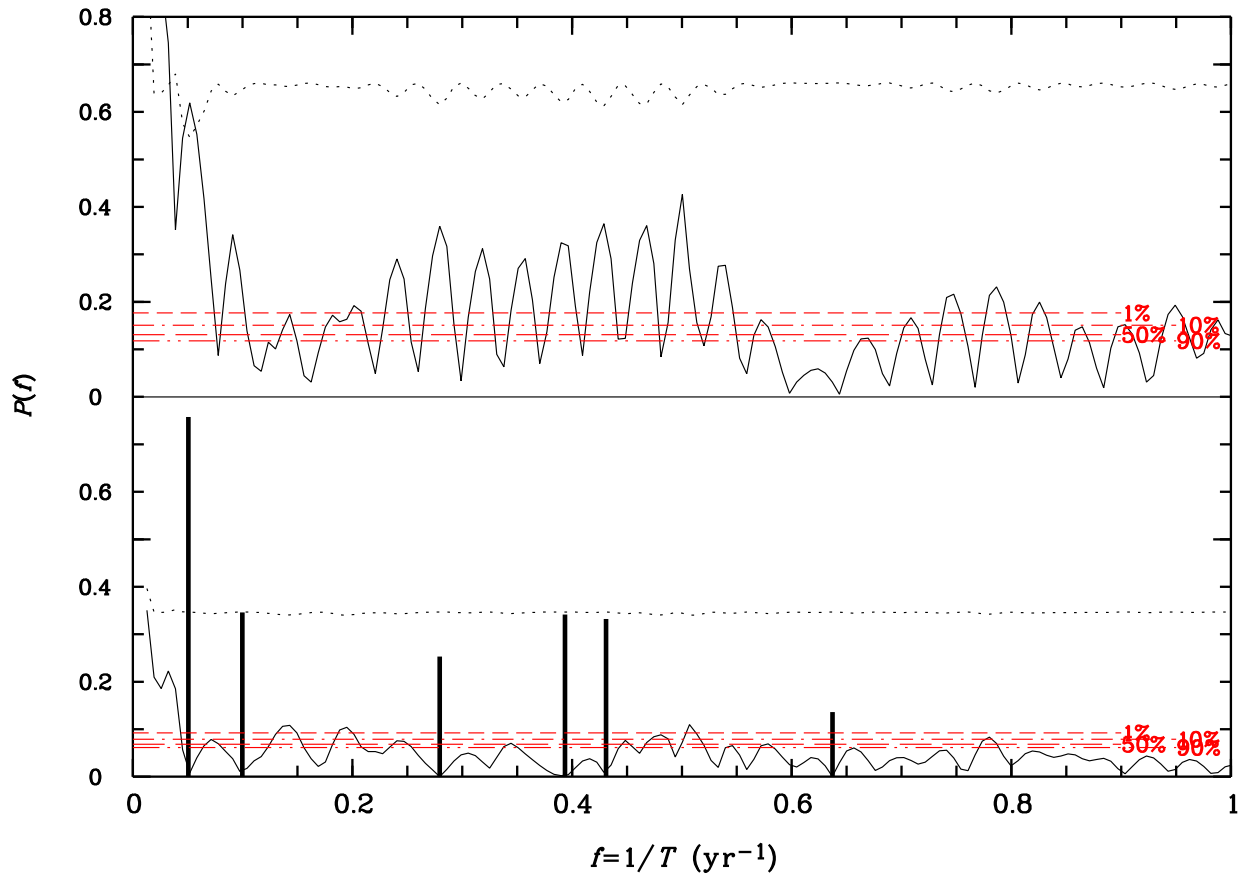


Fig. 10.— As for Fig. 7 but only for the light curve from 1965 – 2004. One *CLEANest* frequency component is beyond the range of the figure.

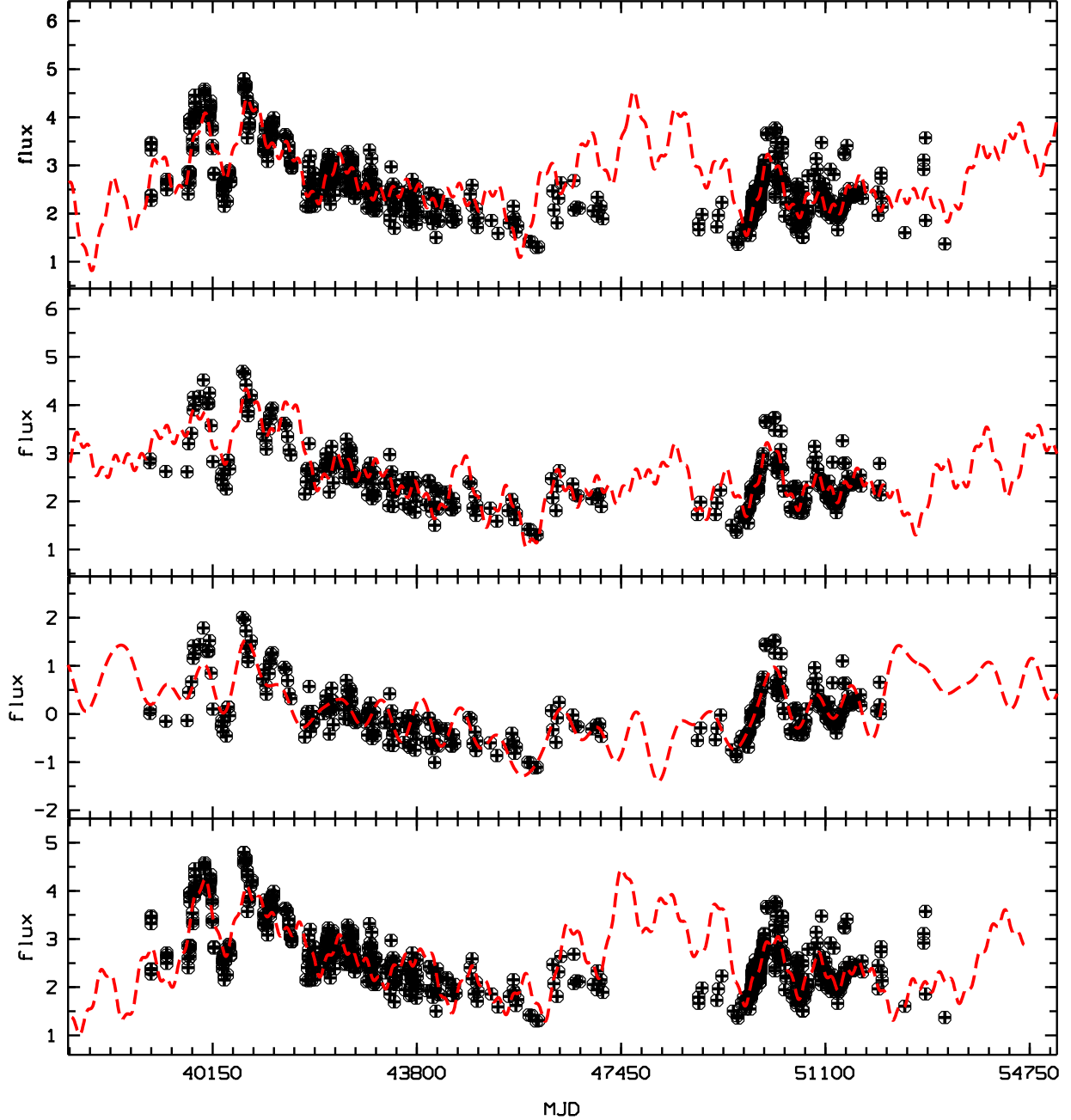


Fig. 11.— Light curves with reconstructions (dashed curves) using *CLEANest* components. From top to bottom the panels show the 1933-2004 V band data, the binned data from the same period, the data with a linear trend removed, and the post 1965 V band data. The dashed curves are the theoretical results obtained by using *CLEANest* components listed in Table 4. For the top 3 panels, only the post 1965 data are plotted for comparison.